



Influence of nozzle geometry on ignition and combustion for high-speed direct injection diesel engines under cold start conditions

J.M. Desantes, J.M. García-Oliver*, J.M. Pastor, J.G. Ramírez-Hernández

CMT Motores Térmicos, Universidad Politécnica de Valencia, Camino Vera s/n, 46022 Valencia, Spain

ARTICLE INFO

Article history:

Received 4 February 2011
Received in revised form 1 June 2011
Accepted 2 June 2011
Available online 22 June 2011

Keywords:

Diesel combustion
Cold start
Injector nozzle
Ignition

ABSTRACT

Starting at low temperatures (below 0 °C) is an important issue for current and near future diesel engine technology. Low ambient temperature causes long cranking periods or complete misfiring in small diesel engines and, as a consequence, an increased amount of pollutant emissions. This paper is devoted to study the influence of nozzle geometry on ignition and combustion progression under glow-plug aided cold start conditions. This study has been carried out in an optically accessible engine adapted to reproduce in-cylinder conditions corresponding to those of a real engine during start at low ambient temperature. The cold start problem can be divided in two parts in which nozzle geometry has influence: ignition and main combustion progress. Ignition probability decreases if fuel injection velocity is increased or if the amount of injected mass per orifice is reduced, which is induced by nozzles with smaller hole diameter or higher orifice number, respectively. Combustion rates increase when using nozzles which induce a higher momentum, improving mixture conditions. For these reasons, the solution under these conditions necessarily involves a trade-off between ignition and combustion progress.

© 2011 Elsevier Ltd. All rights reserved.

1. Introduction

In spite of all the improvements made in diesel technology to date, engine starting is still a problem for current light-duty engines at low ambient temperature and it is a limiting factor for future design trends. Depending on ambient temperature, the starting process of a diesel passenger car engine may result in long cranking periods with a large amount of pollutant emissions [1–4] or in the complete incapability of starting the engine. These problems are caused by poor conditions for auto-ignition: relatively low peak compression temperature and pressure. Low peak compression temperature causes poor vaporization and increases chemical delays. Low peak compression pressure is a consequence of low intake pressure as well as high blow-by level, as a consequence of low engine block temperature and low engine speed. As a reference to poor ignition conditions, Broatch et al. [5] report that a light-duty diesel engine (CR 18:1) can start without aid at temperatures as low as –11 °C. At lower temperatures, ignition aids become necessary. In future applications, in which compression ratio is reduced [6–8] to comply with the near future emissions standards [9,10], starting aids will be necessary at ambient temperatures below 10 °C (tested in a 14:1 CR engine [5]). These facts evidence the necessity of improving knowledge about combustion under low temperature cold start conditions in order to overcome present and future limitations of diesel engines for passenger cars.

During the last decades most of the studies on low temperature cold start have been focused on trial-and-error procedures carried out in climatic chambers [11–14]. These studies have delivered valuable information, but several measurement uncertainties and the inability of using extra diagnostic tools have prevented from making a detailed explanation of this combustion process. Recently, more systematic approaches aiming at engine cold start optimization have been reported. For example, Laget et al. [7] combined in-cylinder pressure analysis, endoscopic visualization and CFD modeling in order to identify the pre-glowing period, nozzle tip protrusion, injector spray angle and cranking speed as key parameters with influence on startability. Perrin et al. [15] presented a more detailed analysis of the combustion sequence in which the location of the first ignition spots are shown to appear in the vicinity of the glow plug, together with the influence of some other parameters like swirl motion and rail pressure. Also, Chartier et al. [16] showed how combustion starts close to the glow plug and does not spread to the whole chamber. All previous papers evidence the current interest of engine community to understand and optimize engine performance under cold start conditions. But most of them address the optimization of a particular engine or vehicle, studying the effect of specific engine parameters on cold start ease. Only few of them try to go deeper into an explanation about the physical mechanisms that control ignition and combustion.

In a previous work by the authors [17], a description of the mechanisms that lead to ignition under cold start conditions was presented as a basis to understand further parametric variations. The study was performed by means of visualization in a

* Corresponding author. Tel.: +34 963877650; fax: +34 963877659.
E-mail address: jgarciao@mot.upv.es (J.M. García-Oliver).

Nomenclature

A	area (m ²)	CCD	charge-coupled device
I	light intensity (-)	CFD	computational fluid dynamics
\dot{m}	mass flow (kg/s)	CMOS	complementary metal oxide semiconductor
\dot{M}	momentum flux (N)	ECU	engine control unit
S	spray penetration (mm)	EOI	end of injection
U	speed (m/s)	EVO	exhaust valve opening
<i>Subscripts</i>		HRL	Heat Release Law
0	conditions at nozzle exit	IL	Integrated Luminosity
<i>cummul</i>	accumulated	IMEP	indicated mean effective pressure
<i>eff</i>	effective	IVC	intake valve closing
<i>f</i>	fuel	LD	Luminosity Delay
<i>Greek symbols</i>		ROHR	rate of heat release
ρ	density	SOC	start of combustion
<i>Abbreviations</i>		SOE	start of energizing
ASOE	after start of energizing	SOI	start of injection
CAD	crank angle degree	TDC	top dead center
		UV	ultraviolet

single-cylinder optical engine that was adapted to systematically reproduce in-cylinder conditions in a real engine at the beginning of the cold starting sequence. The importance of glow plug surface as the only possible ignition spot was confirmed, and it was shown that ignition occurred only after end of pilot injection. For this reason, transport processes that carry the fuel to the glow plug after end of injection were found to be remarkably important. These transport processes can be controlled indirectly by means of rail pressure and injection pulse duration. Furthermore, the injection event was shown to strongly influence combustion progression after ignition.

According to the previous results, it is worth investigating the role of nozzle geometry under cold start conditions, for which no dedicated studies have been found in the literature to date. The aim of the present paper is to show the effect that nozzle geometry has on the mechanisms that lead to ignition and control combustion to validate previous hypotheses and to establish basic criteria for nozzle design and engine optimization. The same experimental setup and methodology as in previous work [17] has been used. A more detailed explanation of the experimental approach can be found in [18]. As additional information for the subsequent analysis of nozzle influence on engine combustion, investigated nozzles have been characterized in terms of mass and momentum fluxes, and mixing evolution has been described by means of non-vaporizing spray visualization tests. After this introduction, the tools and methodology used for the study are presented. Next, the results of nozzle characterization are shown. Later on, the influence of nozzle geometry on ignition and combustion are presented separately. Finally, the main outcomes of this work are summarized.

2. Tools and methodology

2.1. Nozzle characterization tests

To fully describe nozzle performance, two types of hydraulic characterization tests have been carried out: mass flow rate and spray momentum flux. Mass flow rate has been measured in a standard injection rate discharge curve indicator based on the Bosch method [19] (anechoic tub). These tests have been carried out following the same methodology used in [20,21]. Spray momentum flux has been measured in a pressurized chamber filled with

nitrogen, at the same pressure as in the optical engine at SOI. In this test rig, the nozzle is located within this chamber so that one of the sprays impacts on a piezo-electric pressure sensor that has been calibrated to measure force. In this way, the momentum induced by one spray during the stabilized injection period can be measured (transients are not measured properly). To check repeatability, all orifices from the same nozzle have been tested, but only the average value is shown in this paper. A more detailed explanation of the momentum flux measurement test rig and the method principle is shown in references [20,22].

2.2. Non-vaporizing spray visualization

Spray visualization tests were carried out in a constant-volume vessel (the same used in [23,24]) filled with nitrogen at room temperature and at the same density as in the optical engine at SOI. The injector is horizontally mounted and a PixelFly CCD color camera (12 bit – dynamic range) records images through the optical access which is opposite to the injector holder. The PixelFly camera has been used with full resolution of 1280 × 1024 and a flash lamp was used for illumination. For a single injection only one image can be acquired so the spray evolution was scanned by recording images during different injections in 50 μ s intervals, starting at start of injection and finishing when the spray tip reached the limit of field of view. Five repetitions were recorded at each condition to account for injection dispersion. Images were digitally processed using a purpose-developed software which measures maximum spray penetration for each spray in each image. The average value for each time instant is used in this paper. Additional details of the image-processing software are available in reference [25].

2.3. Combustion visualization

2.3.1. Experimental facility

A 4-valve and 0.55 l displacement single cylinder optical engine was used in this study (sketched in Fig. 1). It is equipped with an elongated piston with a cylindrical bowl, with dimensions of 45 × 16 mm (*diameter* × *depth*), which allows optical access to the combustion chamber through a sapphire window placed in its bottom. Below the piston bowl, an elliptical UV mirror is placed on the cylinder axis. In front of the mirror, the high-speed camera

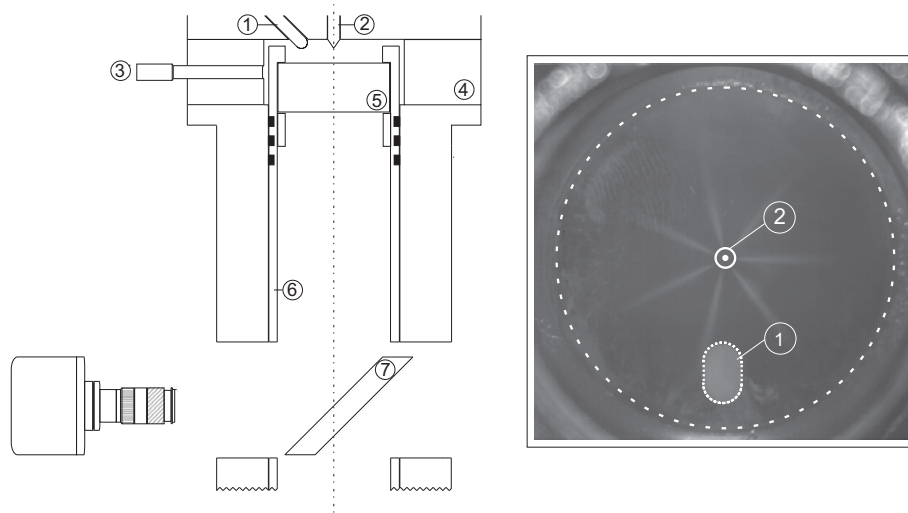


Fig. 1. Sketch of the optical access in the single cylinder engine and an image showing how the combustion chamber is imaged from the camera. 1. Glow plug, 2. Injector nozzle, 3. Pressure transducer, 4. Aluminum piece, 5. Sapphire window, 6. Elongated piston, 7. Elliptical UV mirror.

is positioned to record radiation that comes from the combustion chamber.

The whole facility was adapted, as explained previously in [18], to reproduce the first injection cycle of the starting sequence of a passenger car engine at $-20\text{ }^{\circ}\text{C}$. Specifically, real engine speed and thermodynamic conditions at TDC (temperature and pressure) can be reproduced systematically. Compared to a real transient cold start sequence, the facility makes it possible to perform dedicated studies in which in-cylinder conditions remain unchanged and the independent influence of other parameters can be assessed. Although some phenomena that could play a role on cold start combustion are not reproduced, such as fuel impingement on the extremely cold cylinder walls or the effect of fuel temperature during injection [24], this facility allows to study the combustion process of a glow plug assisted engine under very critical ignition conditions. As a result, several measurements at the same condition can be done to perform statistical analysis, which is specially important due to the high dispersion in the combustion process.

Regarding the reproduced engine conditions, low engine speed (250 rpm) has been achieved by modifying the electronics of the dynamometer. Peak in-cylinder temperature has been reached by reducing compression ratio (from 16:1 to 8:1) and controlling intake temperature at $30\text{ }^{\circ}\text{C}$. Compression ratio has been reduced by placing an aluminum piece (shown in Fig. 1), with 42 mm in height and internal diameter slightly larger than the engine bore, between the cylinder head and the engine block. Peak in-cylinder pressure (27 bar) has been set by controlling intake pressure in a plenum chamber. Besides these conditions, coolant and oil temperatures are also set to $30\text{ }^{\circ}\text{C}$.

A standard glow plug [26] (Fig. 1) was used for the study. At the nominal configuration, the tip protrudes 3 mm into the combustion chamber from the cylinder head plane, it is located at 11.5 mm from the cylinder axis and it is operated at a constant voltage of 11 V.

A common rail injection system with piezo-injectors was operated externally to ensure stable behavior, avoiding uncertainties associated to corrections made by the ECU. The injector is centered in the cylinder and vertically mounted as shown in Fig. 1. In that way, spray orientation with respect to the glow plug can be modified by rotating the injector around its axis. For this study, one of the sprays has been oriented at 12° from the glow plug in swirl direction (swirl ratio: 2.2). Under this configuration, the minimum

distance between the glow plug surface and the spray has been estimated to be 2.3 mm. Injection was performed at a reduced frequency (one injection every 40 cycles) to avoid engine temperature increase, speed instability in case of ignition and to reduce window fouling. Each test consists of 20–30 injection cycles recorded under the same engine conditions.

2.3.2. In-cylinder pressure analysis

The tool employed to perform combustion analysis is the one-zone model CALMEC, which is described in [27]. This diagnosis tool uses the measured in-cylinder pressure as main input. The first law of thermodynamic is applied between IVC and EVO considering the chamber as an open system because of blow-by and fuel injection. The ideal gas equation of state is used to calculate the mean gas temperature in the chamber. Along with these two basic equations, several sub-models are used to calculate instantaneous volume and heat transfer [28], among others. The model main result is the Rate of Heat Release (ROHR). But the temporal evolution of other parameters like the Heat Release Law (HRL, defined as the integral of ROHR and normalized with respect to its maximum) or the mean gas temperature can be calculated. Temporal resolution for these variables depends on the crank angle encoder configuration (0.5 CAD). Global information on each cycle can be obtained, such as Indicated Mean Effective Pressure (IMEP) and Start of Combustion (SOC). SOC is defined as the crank angle position where the beginning of the strong rise in ROHR due to combustion is detected.

2.3.3. Image acquisition and post-processing

Images were recorded using a Photron Ultima APX high-speed camera. It is equipped with a 10-bit CMOS sensor and all images in the study were recorded at an acquisition frequency of 6000 fps to a 512×512 -pixel image size. The camera was coupled with a 135–400 mm focal length Helmut APO objective with a number 1 close up lens.

In order to simplify combustion analysis, time resolved parameters were obtained for every image sequence by means of post-processing. First, segmentation is performed for every single image by calculating a threshold value equal to the minimum digital level in the image (found in a zone without combustion radiation) plus 15% of the difference between the maximum and the minimum. This percentage was chosen as a compromise to eliminate light reflected on the liquid spray and on the chamber walls without

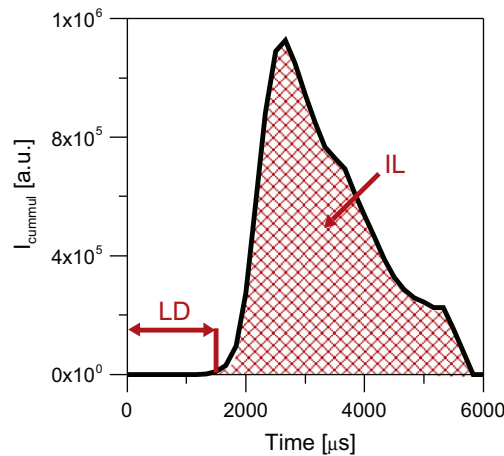


Fig. 2. I_{cumul} as a function of time for a pilot injection test. LD is defined as the time from SOI to flame appearance. IL is defined as the area under the I_{cumul} trace.

losing much information from the combustion event. After segmentation, the digital levels of all pixels containing combustion radiation (with digital levels above the threshold) are added into a single parameter, namely Cumulative Intensity (I_{cumul}). Fig. 2 shows a typical time evolution of this parameter. Additionally pilot probability, Luminosity Delay (LD) and Integrated Luminosity (IL) are used to characterize pilot injection. Pilot probability is defined as the percentage of cycles that show any luminosity out of the whole sample of recorded cycles. As shown in Fig. 2, IL is defined as the integral of the I_{cumul} plot, and LD is the time period between SOI and the first luminosity detection.

2.4. Conditions of the study

Four different multi-orifice micro-sac injector nozzles were selected to carry out the present study and their nominal characteristics are summarized on Table 1. In general, these nozzles are representative of those employed on passenger car diesel engines nowadays. Bosch flow number values range from 250 to 450 cc, number of orifices from 6 to 9 and orifice diameters from 0.121 to 0.145 mm. The differences in included angle can be considered negligible based on the way combustion starts and progresses under these conditions [17]. It has been observed that pilot injection ignites in the glow plug vicinity after end of injection, with a strong influence of flow motion during this period. For this reason, a small variation in glow plug to spray distance induced by differences in included angle (around 0.5 mm) can be considered as negligible. Regarding combustion progression, main combustion develops mainly from pilot flame and due to the negligible influence of included angle on this pilot flame, no major effects are expected of this parameter on main combustion either.

Fuel discharge characteristics for each one of the four nozzles were measured in terms of mass flow rate and momentum flux for two levels of rail pressure, 250 and 370 bar. Mass flow rate

was measured for five different amounts of injected mass (3, 6, 12, 24 and 44 mg) with a constant back-pressure of 27 bar for all cases. Momentum flux was measured in all cases for a single and long injection pulse of 44 mg.

Non-vaporizing spray visualization tests were carried out to investigate spray evolution under two density values. The first one was the same as in the optical engine at TDC (16 kg/m^3), while the second one was 40 kg/m^3 , which is representative of more “conventional” diesel engine operating conditions. In these tests, long injection pulses of 44 mg for each one of the four nozzles and at both levels of rail pressure were tested.

Finally, combustion visualization tests were performed in the optical engine. Basic engine conditions were kept unchanged: engine speed 250 rpm; intake air, oil and water temperature were kept fixed at $30 \text{ }^\circ\text{C}$ and intake pressure was set to reach target peak compression pressure (27 bar). With these engine settings in-cylinder temperature and density were estimated to be $345 \text{ }^\circ\text{C}$ (618 K) and 16 kg/m^3 , which are typical of low temperature cold start cranking process. Two levels of rail pressure were tested, namely 250 and 370 bar. The former one is the lowest possible value for stable behavior at short injection pulses, while the latter one is a value close to the limit above which ignition can not be achieved. The injection strategy consists of two separated pulses, namely 6 mg at 0 CAD and 24 mg at 5 CAD.

3. Nozzle characterization results

3.1. Mass flow rate and momentum flux tests results

Based on flow characterization, this section intends to show how fuel is delivered during the transient period at the beginning of injection, which affects pilot ignition, and during the period when the mass flow rate is completely stabilized, which controls main combustion rate.

For the stabilized injection period, mass flow rate and momentum flux results are shown in Figs. 3 and 4, respectively. In both figures, results for the four nozzles at both levels of rail pressure and for a long single injection of 44 mg are presented. Fig. 3 shows how the mass flow rate traces reach a maximum stabilized period according to the Bosch flow number values given in Table 1. Nozzles N3 and N4 reach the highest mass flow rate, followed closely by nozzle N2. Nozzle N1 is considerably different, this nozzle reaches a maximum mass flow rate value which is around the half of those reached by nozzles N3 or N4. As a consequence, the injection time is considerably longer for nozzle N1, if the amount of injected mass is the same. Fig. 4 shows the total stabilized momentum flux and the effective area per orifice calculated according to:

$$A_{eff} = \dot{m}_0^2 \div (\dot{M}_0 * \rho_f) \quad (1)$$

where ρ_f is the fuel density, \dot{m}_0 and \dot{M}_0 are the mass flow rate and momentum flux per orifice, respectively, during the stabilized period. The total stabilized momentum flux (number of orifices times \dot{M}_0) is an important parameter which promotes mixing during main combustion. A_{eff} values in Fig. 4 agree with nominal area values calculated with nominal diameters from Table 1, and they will be used to estimate fuel velocity during the transient injection period.

For the transient injection period, Fig. 5 shows the mass flow rate per orifice for a single pilot injection pulse of 6 mg, for the four nozzles and at both levels of rail pressure. Mass flow rate per orifice is selected, since pilot ignition is the result of the interaction between the glow plug and only one of the sprays. It must be taken into account that the amount of fuel injected per orifice is different among nozzles depending the number of holes, since the injection strategy maintains a constant total injected mass. From the results in Fig. 5 it is clear that the mass flow rate traces never reach

Table 1
Nominal characteristics of the four multi-orifice injection nozzles selected for the study.

Nozzle	N1	N2	N3	N4
Number of orifices (-)	6	6	7	9
Bosch flow number (cc/30 s 100 bar)	250	400	450	450
included angle ($^\circ$)	155	150	153	153
Diameter (mm)	0.121	0.145	0.142	0.125
K-factor (-)	0	1.5	1.5	1.5

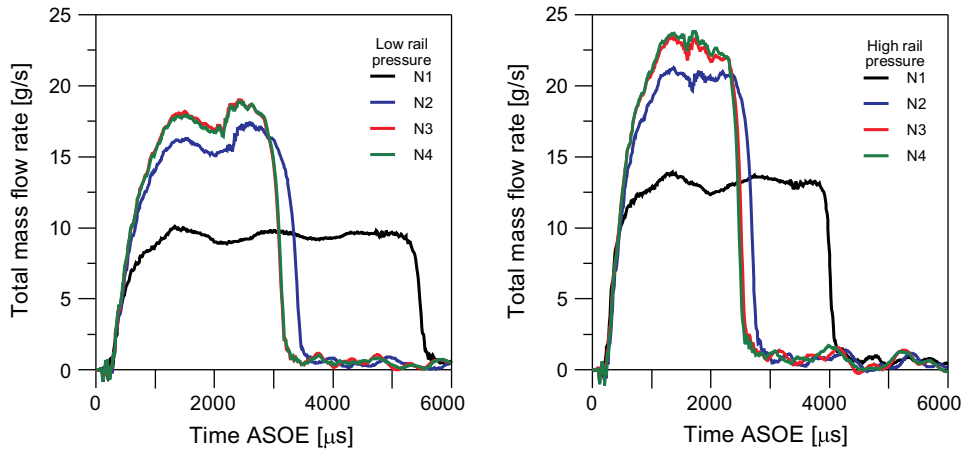


Fig. 3. Fuel mass flow rate as a function of time for each of the nozzles tested with a single injection strategy of 44 mg at both levels of rail pressure.

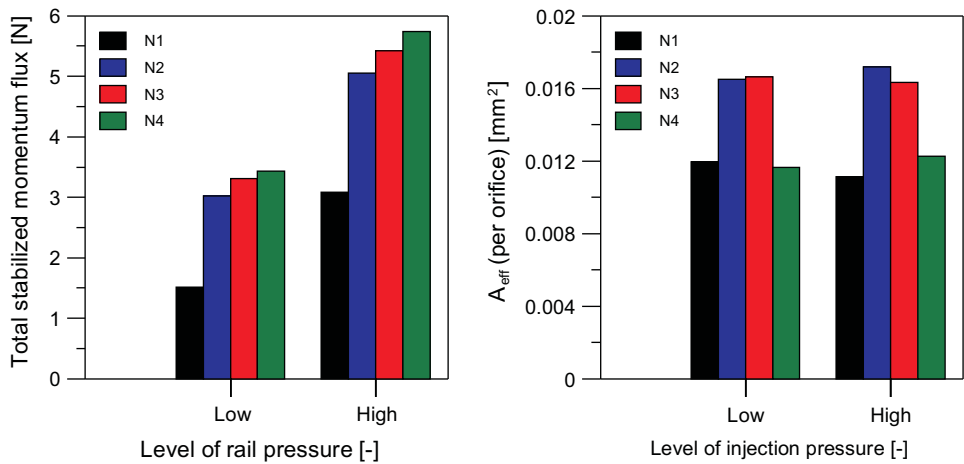


Fig. 4. Total stabilized momentum flux (measured momentum flux times the number of orifices) and A_{eff} at both levels of rail pressure for the four nozzles.

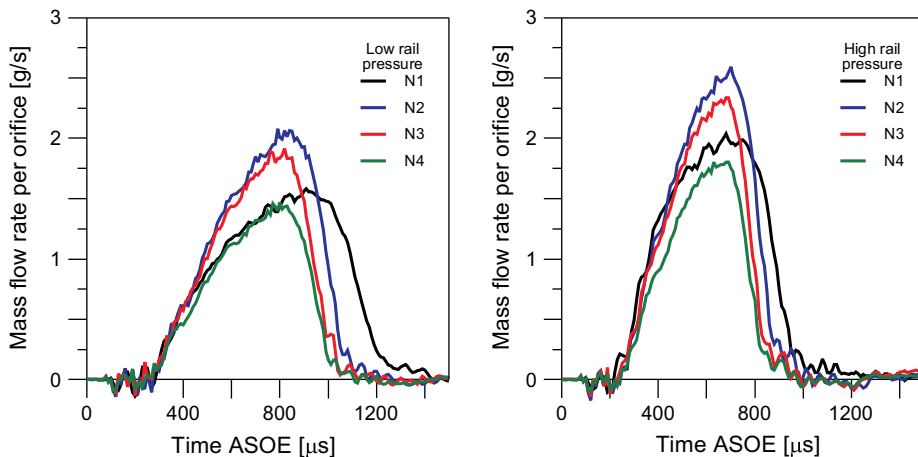


Fig. 5. Mass flow rate per orifice as a function of time ASOE for the four nozzles tested at both levels of rail pressure.

stabilization under these conditions and pilot injection is a completely transient event. Differences in mass flow rate among nozzles are smaller in comparison with differences in total mass flow rate under stabilised conditions (Fig. 3).

Reliable momentum flux measurements during transients are not possible. Therefore, in order to characterize pilot injection, maximum fuel speed for these short pulses has been

estimated. This parameter will be used as an indicator for the intensity of the fuel velocity after EOI and, which has been shown to have a strong influence on pilot ignition [17]. Effective injection speed (U_{eff}) has been calculated according to the following equation:

$$U_{eff} = \dot{m}_0 \div (A_{eff} * \rho_f) \tag{2}$$

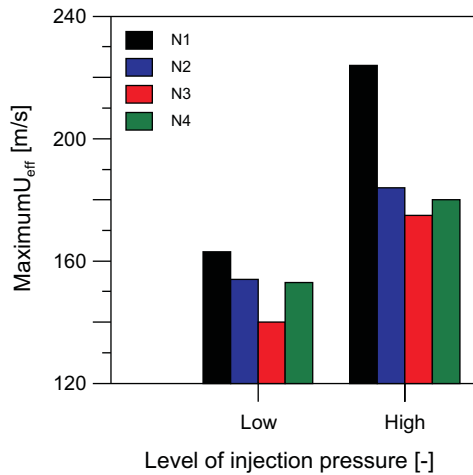


Fig. 6. Estimated maximum fuel speed reached during pilot injection for the four nozzles, at both levels of rail pressure and for single injection of 6 mg.

where \dot{m}_0 is the measured mass flow rate per orifice (Fig. 5), ρ_f is the fuel density and A_{eff} is the effective nozzle area. The latter parameter is assumed to be constant and equal to the area calculated during the stabilized period (Fig. 4). From the time evolution of the injection velocity, the maximum value is used as a characteristic parameter. A similar approach has been followed in [29] and it is considered quite acceptable for micro-sac nozzles. The estimated maximum fuel speed is plotted in Fig. 6 for the four nozzles at both levels of rail pressure for a single injection of 6 mg. The maximum speed reached by nozzle N1 is clearly higher than that by any of the other three nozzles. Nevertheless, a direct comparison must be done only with nozzle N2, with the same amount of injected fuel per orifice. The difference between both nozzles could be due to the fact that the transient period at start of injection is faster for N1, and therefore injection rate is closer to stabilization for this nozzle. Maximum fuel speed values for nozzles N2, N3 and N4 are very similar. But it must be noted that differences in fuel speed are due not only to the specific geometry of each nozzle, but also to a different amount of injected mass per orifice.

3.2. Non-vaporizing spray visualization results

Injections were performed into a volume filled with nitrogen at the same density as in the engine at TDC (16 kg/m^3) and at a higher

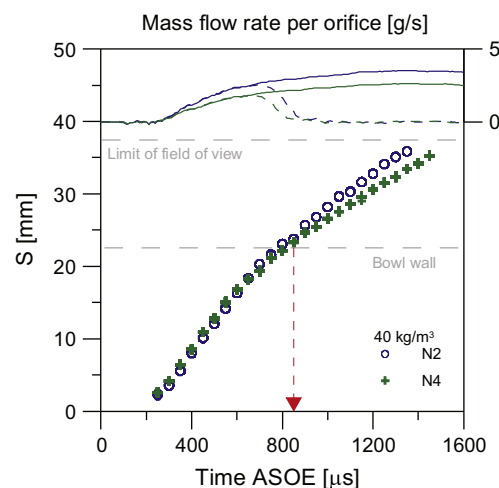
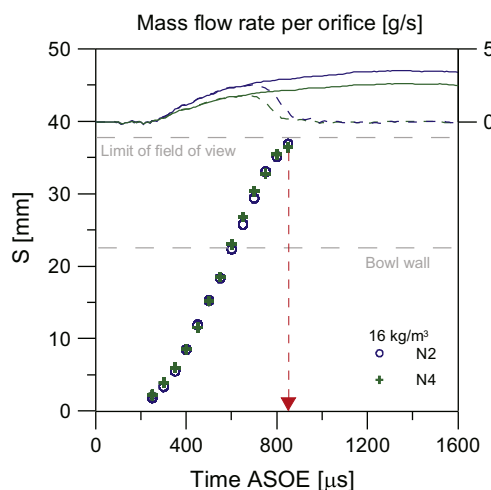


Fig. 7. Spray penetration as a function of time for nozzles 2 and 4 at the high level of rail pressure for two different densities, 16 kg/m^3 (left) and 40 kg/m^3 (right). Mass flow rate for a long and a pilot injection are plotted at the top of each graph. Additionally, the limit of the field of view and the bowl wall distance are indicated with dashed lines.

density (40 kg/m^3) representative of “conventional” diesel engine operating conditions. Long injection pulses are used to identify spray penetration, although this information can also be used to analyze short pulses, at least until EOI. A representative example of the results is shown in Fig. 7. For clarity, only two nozzles with different orifice diameter are shown (N2 and N4), at the high level of rail pressure and for both density values. Spray penetration is plotted against time, and mass flow rates are also shown as a reference of the injection event. For the low density case, spray penetrates linearly (with respect to time) reaching the bowl walls distance within a very short time. No differences between nozzles have been detected in spite of having very different orifice diameters. This lack of dependence can be better understood by looking at the high density case, for which two periods can be differentiated. From SOI until approximately $800 \mu\text{s}$, the spray penetrates quasi-linearly with no differences between nozzles, as in the low density case. But after that, penetration evolution proceeds at a slower rate (approximately with the square root of time). Differences start to arise and spray penetration is notably higher for nozzle N2 in this second period. In fact, this is the logical trend since N2 has the largest orifice diameter as reported previously by Naber and Siebers [30]. The duration of the first period corresponds approximately to the time for injection rate stabilization, and is similar for both ambient densities, as the injection rate is approximately the same. However, the spray reaches the field of view limit at the end of the first period in the low density case. For this reason, it is not possible to analyze trends after that point. Anyway, the bowl wall distance has been reached much earlier in the injection process, and therefore no differences can be expected during engine tests in free spray evolution. It can be concluded that, at low density conditions and with small combustion chambers (as in passenger car engines cold start), there is almost no difference in spray penetration for nozzles investigated. This means that the time for the spray to reach the glow plug or the bowl walls is practically the same for all nozzles.

4. Nozzle influence on pilot ignition

Previous work by the authors [17] has shown that pilot ignition can only be monitored by means of visualization, since the effect of pilot combustion on the ROHR trace is on the noise level. Experimental results have shown that ignition of pilot injection occurs solely close to the glow plug, where high temperature ensures a reasonable ignition delay. Vaporization process is very slow, and only a small amount of fuel vapor reaches the glow plug during

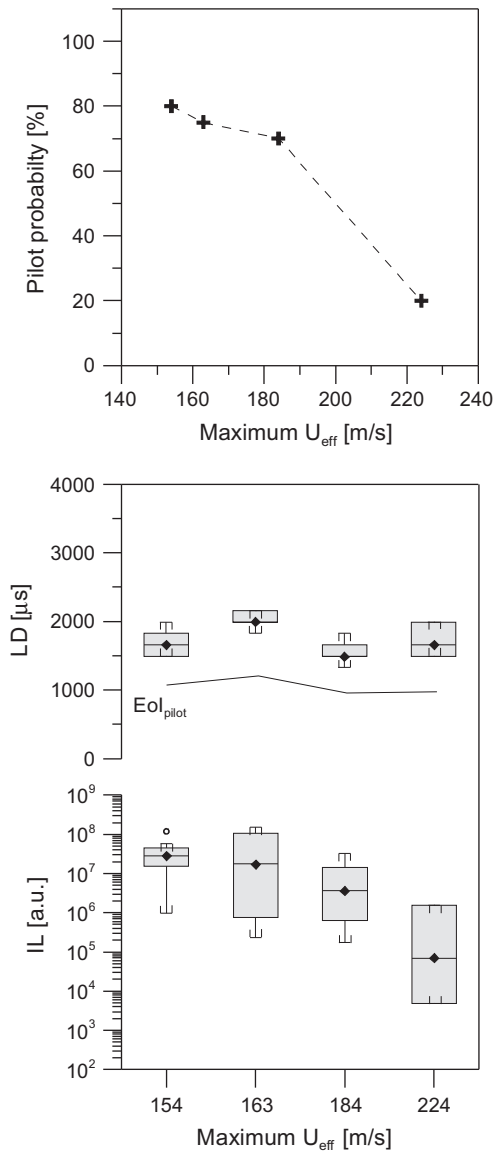


Fig. 8. Pilot probability (top), LD (middle) and IL (bottom) as a function of maximum fuel speed at both levels of rail pressure, for nozzles N1 and N2 with a constant injection strategy of 6 mg at TDC. On the LD graph, a line representing EOI is plotted as a reference of the injection event.

the injection event due to the low air temperature within the chamber. After end of injection, residual flow together with transient air entrainment create a peak in equivalence ratio close to the glow plug area, which is favorable for combustion initiation. This peak is higher at low rail pressure and for shorter injections.

This sub-section aims to shed some light the controlling mechanisms of pilot injection ignition. For analysis purposes, results from visualization of tests where a single pilot injection has been performed are grouped according to the amount of fuel injected per orifice. For all nozzles, a total mass of 6 mg has been injected. According to differences in number of holes, nozzles N1 and N2 inject the same amount of fuel per orifice, while nozzles N2, N3 and N4 will make it possible to study the effect of changing the amount of injected mass per orifice.

4.1. Ignition at constant injected mass per orifice

Pilot injection results are analyzed in this sub-section for nozzles N1 and N2 at a constant injected mass per orifice of 1 mg.

These results are shown in Fig. 8 in terms of pilot probability, LD and IL as a function of maximum fuel speed, since nozzle characterization results have shown that the main effect of nozzle geometry and rail pressure observed in the investigated nozzles is a change in the speed at which fuel is delivered. Specifically, the maximum value of this speed has been chosen as a reference one. Results evidence that pilot probability and IL depend on fuel speed. Actually, both pilot probability and IL are observed to drastically decrease when fuel speed is increased. Besides, LD does not depend on fuel speed, while it seems to correlate with EOI, since the time between EOI and the appearance of the first flame spots is very similar for these four different injection conditions.

The present results agree with previous trends reported in [17] for a single nozzle where an increase of rail pressure was shown to decrease both ignition probability and IL. Under those conditions, pilot mass was kept constant when changing rail pressure (i.e. higher fuel velocity). Present results hint at the fact that changing fuel velocity by modifying either rail pressure or nozzle geometry

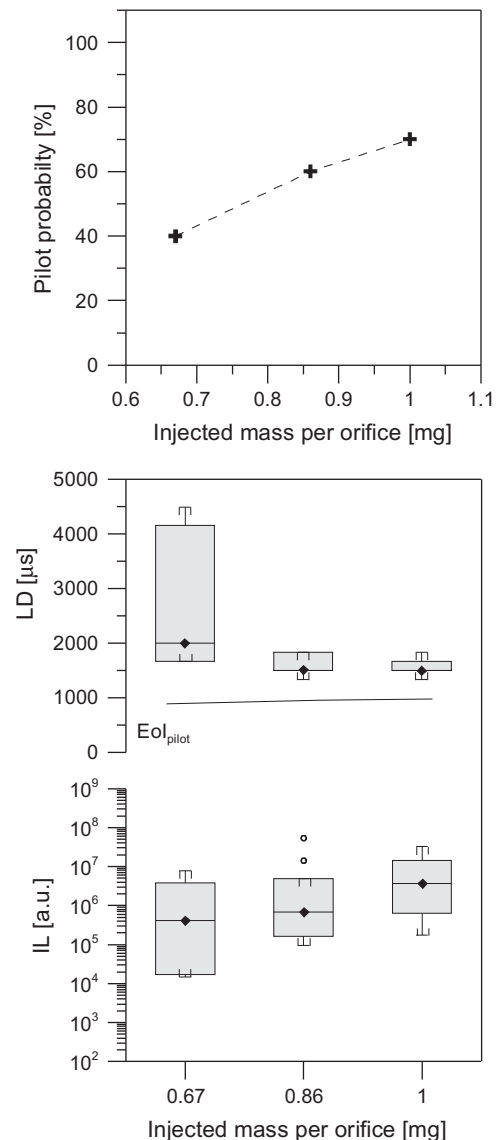


Fig. 9. Pilot probability (top), LD (middle) and IL (bottom) as a function of injected mass per orifice. These results correspond to a rail pressure of 370 bar, for a single injection pulse of 6 mg for the nozzles N2, N3 and N4. On the LD graph, a line representing EOI is plotted as a reference of the injection event.

have similar consequences. It also reinforces the hypothesis shown in [17] that an increase in fuel velocity increases the amount of fuel that reaches the piston wall, reducing the equivalence ratio close to the glow plug.

4.2. Influence of injected mass per orifice

Pilot injection results are analyzed in this section for nozzles N2, N3 and N4 at a constant total injected mass of 6 mg. Fig. 9 shows pilot probability, LD and IL as a function of the injected mass per orifice at the high level of rail pressure. Increasing injected mass per orifice, under these conditions, has a positive effect on the appearance probability of the pilot flame and on flame intensity (IL). Regarding LD, no large variation is observed when increasing the injected mass per orifice. In agreement with previous sub-section, the time between EOI and the first appearance of flame seems to remain constant for these three nozzles. These results hint at the fact that increasing injected mass per orifice with similar maximum fuel speed improves conditions for ignition noticeably due to an increasing equivalence ratio in the glow plug vicinity.

Results showed in this section have allowed to isolate the positive effect of increasing the amount of injected mass per orifice and the negative effect of increasing the fuel speed during the injection event. These two effects are combined when the total pilot injection mass is increased keeping the injection nozzle and rail pressure the same, which has been previously reported in [17]. Under such conditions, it was shown that increasing the total pilot injected mass made autoignition more difficult, delayed the apparition of flame and diminished the amount of light radiated by burning fuel. The present results indicate that the negative effect of increasing fuel speed is more important than the positive effect of increasing the amount of injected mass per orifice, which must

be taken into account when selecting injection strategies for real engine cold start.

5. Nozzle influence on main combustion

Fig. 10 illustrates the main combustion development for a pilot + main injection strategy under cold start conditions. A combustion cycle of nozzle N1 at low rail pressure has been selected as a representative example. Main combustion starts when the spray closest to the glow plug reaches the pilot flame. From here on, combustion progresses by burning the fuel injected by this spray and later on propagating to the adjacent sprays. As injection finishes, the visible flame stops propagating, indicating that injection is the main promoter of the combustion progress. This sequence shows that cold start combustion can be divided into two problems: ignition and main combustion progress progress. Ignition is promoted by pilot flame and controlled by parameters studied in the previous section. Combustion progress is controlled by the main injection event.

Fig. 11 evidences the relationship between pilot flame and main combustion for the conditions investigated in the present paper. Combustion probability (IMEP higher than zero) of full injection tests is plotted versus flame appearance probability (IL higher than zero) measured in tests with the same pilot injection strategy but without the main pulse. It must be noted that full and pilot injection results stem from in-cylinder pressure analysis and flame visualization, respectively. Although the match is not completely perfect, the information given in this figure proves that pilot ignition clearly influences the full-strategy success for the conditions tested. The higher the pilot probability, the higher the main combustion probability. Additionally, the strong influence of rail pressure is also shown in this figure, as high pilot and main combustion probability are achieved at low rail pressure.

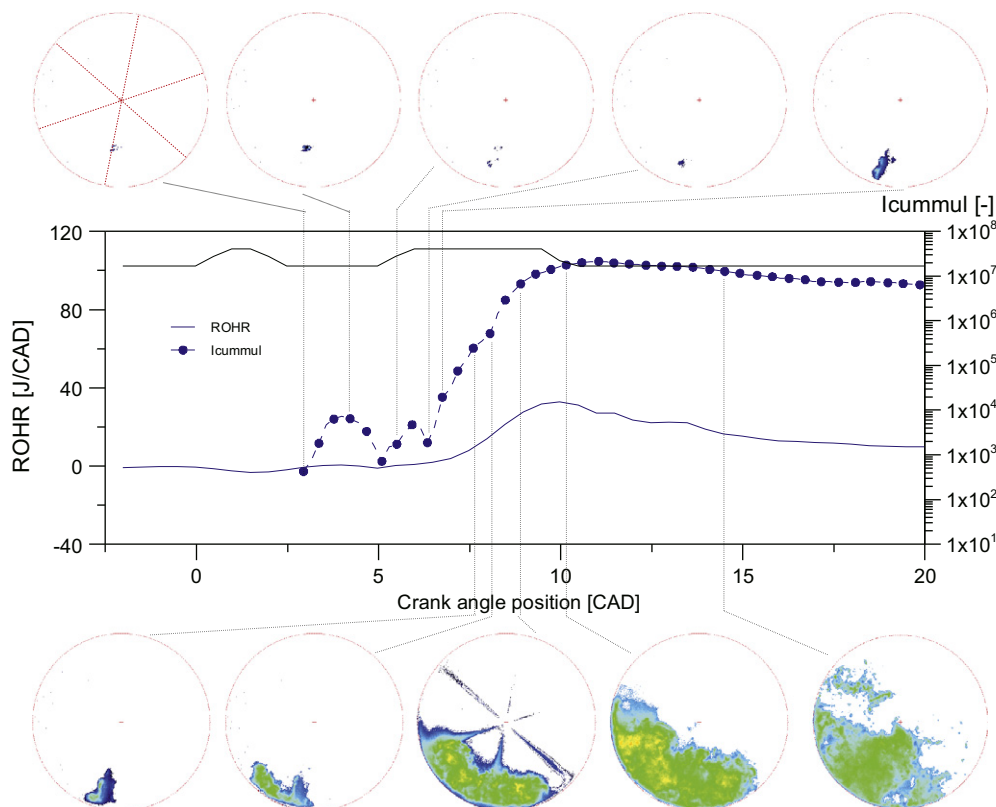


Fig. 10. Injection pulse, ROHR and I_{cummul} as a function of the crank angle position together with selected images of a combustion cycle at the low level of rail pressure for nozzle N1, pilot injection of 6 mg injected at 0CAD and main pulse of 24 mg at 5 CAD. Radial lines on the top left image correspond to the approximate locations of the sprays.

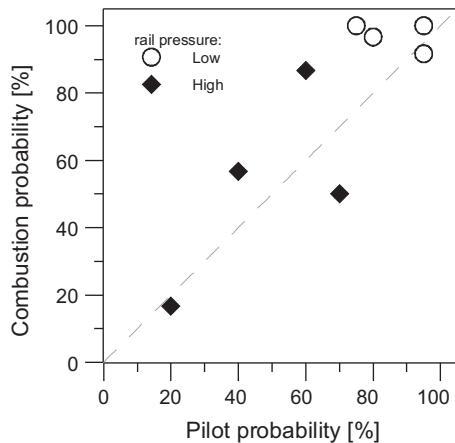


Fig. 11. Combustion probability (IMEP higher than zero) for full injection tests as a function of the pilot flame probability (IL higher than zero) for the four nozzles and both levels of rail pressure.

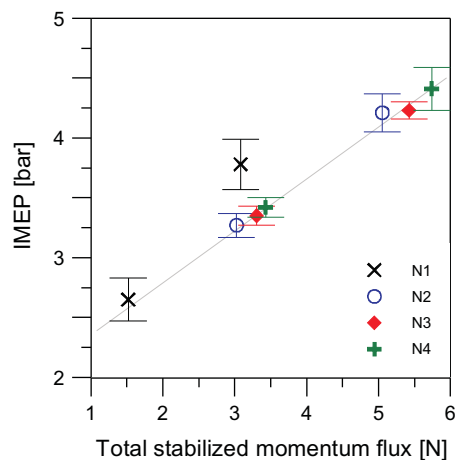


Fig. 12. Average IMEP for cycles with positive work of 30 repetitions tests as a function of the momentum multiplied by the number of orifices. The confidence interval of the mean (with a confidence level of 95%) is plotted with error bars. Both levels of rail pressure are plotted for the four nozzles.

Regarding the fact that injection is the main combustion promoter, it was also reported in [17] that increasing rail pressure has a positive effect on IMEP, probably due to a higher momentum induced by the injection event that enhances mixing process. This statement can be confirmed from Fig. 12, which shows IMEP as a function of the total stabilized momentum flux (Fig. 4). Conditions correspond to full-strategy combustion tests for the four nozzles and both levels of rail pressure. IMEP is calculated from cycles with positive work out of a 30 repetition test. The plot somehow collapses results from the different nozzles. Increasing total momentum flux results in an increase in IMEP, which can be achieved by increasing momentum flux per orificie (i.e. by increasing injection pressure or nozzle diameter, nozzles N1 and N2) or by increasing the number of orifices. In both cases, the effect on IMEP is positive, most probably due to the intimate positive link between momentum flux and mixing and vaporization processes, which enhances combustion propagation. Consequently, high momentum values are desirable to improve combustion process under cold start conditions.

6. Summary and conclusions

A study on the influence of injector nozzle geometry on ignition and combustion progress under cold start conditions has been

presented. This study has been carried out in a specially adapted facility which allows to reproduce, repetitively and in a systematic manner, low speed and low temperature conditions such as those achieved by a passenger car diesel engine at -20°C . In this facility, classical in-cylinder pressure analysis can be coupled with high-speed visualization which has allowed more insight to be gained into the ignition and combustion progression controlling mechanisms.

For conditions under investigation, it has been shown how combustion initiation is promoted, almost exclusively, by pilot injection flame. This clear dependence allowed the combustion problem to be split in two parts: ignition and main combustion progress. Ignition is controlled by pilot injection and can only be monitored by means of visualization. Main combustion progress is promoted by the injection event, and can be monitored with classical in-cylinder pressure analysis, as well as with combustion visualization.

Two parameters have been shown to have a clear influence on pilot ignition: injected mass per orifice and speed. Increasing the amount of fuel injected per orifice at similar fuel speed, improves conditions for ignition probably by carrying a larger amount of fuel to the glow plug and increasing the local equivalence ratio. Increasing fuel speed reduces ignition probability considerably by carrying a larger amount of fuel towards the piston wall away from the glow plug. For this reason, conditions for pilot ignition are enhanced at low rail pressure and/or by using short injection pulses.

Regarding main combustion progress, a positive dependence has been found between momentum induced by the injection event and the amount of work obtained per cycle. For this reason, increasing rail pressure is desirable during main combustion. All in all, both single pilot and full injection results lead to the conclusion that a compromise must be made, at least under these conditions, to find optimum settings for both ignition and combustion progress.

Acknowledgements

Authors thank the Spanish Ministry of Innovation and Science for the financial support through the project OPTICOMB (reference code: TRA2007-67961-C03-C01). Authors also thank Daniel L rida S nchez de las Heras for his outstanding work in the facility set-up and adaptation and for his support during the tests.

References

- [1] Yassine MK, Tagomori MK, Henein NA, Bryzik W. White smoke emissions under cold starting of diesel engines. SAE Paper 960249; 1996.
- [2] Peng H, Cui Y, Shi L, Deng K. Effects of exhaust gas recirculation (egr) on combustion and emissions during cold start of direct injection (di) diesel engine. Energy 2008;33(3):471–9. doi:10.1016/j.energy.2007.10.014.
- [3] Peng HY, Cui Y, Deng HY, Shi L, Li LG. Combustion and emissions of a direct-injection diesel engine during cold start under different exhaust valve closing timing conditions. Proc Inst Mech Eng, Part D: J Automobile Eng 2008;222(1):119–29.
- [4] Weilenmann M, Favez J, Alvarez R. Cold-start emissions of modern passenger cars at different low ambient temperatures and their evolution over vehicle legislation categories. Atmos Environ 2009;43(15):2419–29.
- [5] Broatch A, Ruiz S, Margot X, Gil A. Methodology to estimate the threshold in-cylinder temperature for self-ignition of fuel during cold start of diesel engines. Energy 2010;35:2251–60.
- [6] Pacaud P, Perrin H, Laget O. Cold start on diesel engine: is low compression ratio compatible with cold start requirements? SAE Paper 2008-01-1310; 2008.
- [7] Laget O, Pacaud P, Perrin H. Cold start on low compression ratio diesel engine: experimental and 3D RANS computation investigations. Oil Gas Sci Technol Rev IFP 2009;64(3):407–29.
- [8] MacMillan D, La Rocca A, Shayler PJ, Murphy M, Pegg IG. The effect of reducing compression ratio on the work output and heat release characteristics of a DI diesel under cold start conditions. SAE Paper 2008-01-1306; 2008.
- [9] Johnson TV. Review of CO₂ emissions and technologies in the road transportation sector. SAE paper. 2010-01-1276; 2010a. doi:10.4271/2010-01-1276. <http://papers.sae.org/2010-01-1276>.

- [10] Johnson TV. Review of diesel emissions and control. SAE paper. 2010-01-0301; 2010b. doi:10.4271/2010-01-0301. <<http://papers.sae.org/2010-01-0301>>.
- [11] Payri F, Broatch A, Serrano JR, Rodríguez LF, Esmoris A. Study of the potential of intake air heating in automotive DI diesel engines. SAE paper 2006-01-1233; 2006.
- [12] Henein NA, Zahdeh AR, Yassine MK, Bryzik W. Diesel engine cold starting: combustion instability. SAE paper 920005; 1992.
- [13] Zahdeh AR, Henein NA, Bryzik W. Diesel cold starting actual cycle analysis under border-line conditions SAE paper 900441; 1990.
- [14] Osuka I, Nishimura M, Tanaka Y, Miyaki M. Benefits of new fuel injection system technology on cold startability of diesel engines improvements on cold startability and white smoke reduction by means of multi injection with common rail fuel system (ECD-U2). SAE paper 940586; 1994.
- [15] Perrin H, Dumas JP, Laget O, Walter B. Analysis of combustion process in cold operation with a low compression ratio diesel engine. SAE paper 2010-01-1267; 2010.
- [16] Chartier C, Aronsson U, Andersson Ö, Egnell R. Effect of injection strategy on cold start performance in an optical light-duty DI diesel engine. SAE paper 2009-24-0045; 2009.
- [17] Pastor JV, García-Oliver JM, Pastor JM, Ramírez-Hernández JG. Ignition and combustion development for high speed direct injection diesel engines under low temperature cold start conditions. Fuel 2011;90(4):1556–66.
- [18] Pastor JV, García-Oliver JM, Pastor JM, Ramírez-Hernández JG. Experimental facility and methodology for systematic studies of cold startability in direct injection diesel engines. Meas Sci Technol 2009;20(095109). doi:10.1088/0957-0233/20/9/095109.
- [19] Bosch W. The fuel rate indicator: a new measuring instrument for display of the characteristics of individual injection. SAE paper 660749; 1966.
- [20] Payri R, García JM, Salvador F, Gimeno J. Using spray momentum flux measurements to understand the influence of diesel nozzle geometry on spray characteristics. Fuel 2005;84:551–61.
- [21] Payri R, Salvador FJ, Gimeno J, Bracho G. A new methodology for correcting the signal cumulative phenomenon on injection rate measurements. Exp Tech 2008;31(1):46–9.
- [22] Payri R, Salvador F, Gimeno J, Zapata L. Diesel nozzle geometry influence on spray liquid-phase fuel penetration in evaporative conditions. Fuel 2008;87:1165–76.
- [23] Pastor J, Payri R, López JJ, Julia JE. Effect of injector nozzle geometry of diesel engines on the macroscopic spray characteristics by means of optical techniques. In: Transactions 2003-2 of IMechE two day conference on fuel injection systems. London: Professional Engineering Publishing; 2002. p. 73–82.
- [24] Payri R, Salvador F, Gimeno J, Bracho G. Effect of fuel properties on diesel spray development in extreme cold conditions. Proc Inst Mech Eng, Part D: J Automobile Eng 2008;222(9):1743–53.
- [25] Pastor J, Arrégle J, García J, Zapata L. Segmentation of diesel spray images with log-likelihood ratio test algorithm for non-gaussian distributions. Appl Optics 2007;46(6):888–9.
- [26] Lindl B, Schmitz H. Cold-start equipment for diesel direct-injection engines. SAE paper 1999-01-1244; 1999.
- [27] Payri F, Molina S, Martín J, Armas O. Influence of measurement errors and estimated parameters on combustion diagnosis. Appl Therm Eng 2006;226–36.
- [28] Torregrosa A, Olmeda P, Degraeuwe B, Reyes M. A concise wall temperature model for di diesel engines. Appl Therm Eng 2006(26):1320–7.
- [29] Payri R, Salvador FJ, Gimeno J, De la Morena J. Influence of injector technology on injection and combustion development v part 1: Hydraulic characterization. Appl Energy 2011;88(4):1068–74.
- [30] Naber JD, Siebers DL. Effects of gas density and vaporization on penetration and dispersion of diesel sprays. SAE paper 960034; 1996.